Journal of New Technology and Materials (JNTM)
J. New Technol. Mater.
Vol. 07, N°02 (2017)47-55

OEB Univ. Publish.Co.

Theoretical investigation of δ-doped double barriers GaAs/AlGaAs RTDs at varying device geometry and temperature dependence

Man Mohan Singh[a], M. J. Siddiqui[a] and P. A. Alvi[b]

[a]*Department of Electronics Engineering, Aligarh Muslim University, Aligarh, UP-202002, India*

[b]*Department of Physics, Banasthali University, Banasthali-304022, Rajasthan, India*

Corresponding author: email: macky4589@gmail.com

Received date: Jul 28, 2017; accepted date: Dec 16, 2017

Abstract

In this article, we proposed a new concept of Si-delta doping in double barrier resonant tunneling diode heterostructure. The double barrier resonant tunneling diodes (DBRTDs) are investigated through the technique of contact block reduction (CBR) incorporating nonequilibrium Green's function (NEGF) of a quantum structure in ballistic limits. This paper addresses the diverse characteristics of DBRTDs with variation in device parameters like barriers length, doping concentration and spacer layer. Dependence of operating temperature with the device geometry is also mentioned along with variation of Si-delta doping. Sharp delta doping of 1nm splits the well in two parts and study of current ratios and current density Jₚ. Improvement in the performance of this semiconductor device has been utilized by this study with different device parameters. Furthermore, the comparison of these electrical properties with existing devices provide effective relation of Negative differential resistance (NDR), current ratio, conductance and band gap with device parameters variations which provide abilities of this device to ostentatious the functionality. Nextnano3 tool provide these characteristics and validate them with experimental research work existing in the literature survey.

Keywords: NEGF, Peak to valley current ratio (PVCR), Ballistic limits, Delta Doping, device Simulation.

1. Introduction

In recent decades, quantum devices are the key factors for achieving ultra-high speed and ultra-high frequencies (in THZs). GaN based DBRTDs provides the stability at both ends of resistivity by changing the polarity of biasing [1]. Enhancement in the characteristics of the device has been included with the insertion of Silicon delta doping, which is useful for any device as it synthesizes easily [2]. Moreover, quantum physics may work smarter over classical when integrate with new devices at the dimension of nanometers. Tunneling based quantum devices including charge quantization and hot electron injections have been analyzed for decades, mostly using semiconductor III-V materials [3]. Study of luminescence excitation mechanisms can also be done by DBRTDs. Instantaneously, the probability of excitation formation can be offered by them while injection of a low density electron and hole into the quantum well simultaneously [4-5]. In context to MOS based transistor devices, parasitic effects are mainly due to quantum effects which degrade the efficiency and boundary limits in the operation of device working. Indeed, degradation of coupling between gate and channel is dependent of confinement of quantum devices [6], increment in power consumption responds due to tunneling electron through the gate [7] and basic limitation of operation in MOS transistor is due to tunneling through source to drain [8].

In quantum devices, Double Barrier Resonant tunneling diode is one of the most encouraging for low power consumption, ultra-high speed and ultra-high frequency devices. This device works on the operation of tunneling under quantum effect. Characteristics of the DBRTD give more favorable at low voltage and as well as at low power. In present years, DBRTDs have widely considered due to very high speed of operation and reduced complexity with increased functionality along with consumption of low power due to its feature of negative differential region [9]. Reduced circuit complexity is due to enhancements in progress of fabrication technologies and use of the single gate instead of bipolar and MOS circuits [10-11]. The device structure is the most important factor for modelling and characterization of DBRTD. We are varying the barrier lengths, doping concentration and alloy concentration of the device and brighten that how these parameters are pretentious the characteristics of the device and how the peak to valley ration (PVCR) changes with doping concentration and barrier length. DBRTDs exhibit the negative resistance behaviour which is useful in circuit based on digital memory. We also deliberate the outcome of barrier length and concentration through the NDR region of the device which gives us better results for digital

circuits.

Any quantum device can't be modeled without considering the operating temperature as a main feature for its manufacturing and designing of micro-electronic circuits [12-13]. Suggestively, if we want to alter the characteristics of any quantum device, temperature changes of few kelvins can do this at nanoscale [14-15]. For a good device, structural characteristics for entire range of temperature give good performance of any quantum device. Reliability of any device at very high frequency is required to give the high performance at extremes of the temperature [16-17].

In this research paper, we are expending the AlGaAs/GaAs DBRTD and calculate the properties and we have also analyzed this device with Si-delta doping at the center of the quantum well. To achieve accurate results for application at terahertz frequencies, we have to assume momentum be parallel for carrier transport. Besides this, fabrication of resonant tunneling diode on integrated circuits for millimeter wave devices has been done with film diode technology with low lost at compact designing. For radiation and imaging systems, we have some application in the field of biomedical technology.

The organization of remaining article is given as follows. Section II discusses the estimation detail of device parameters with simulation software. Section III discusses the mathematical and operational details. Section IV describes the proposed device structure. Electrical and simulation activity are described in fifth section. Finally, VI Section concludes the paper.

2. Estimation Details

Environment provided for simulation of semiconductor devices and characterizes the heterostructure with the basic bodily properties of real 1D, 2D and 3Drealisticstructure has been provided in the Nextnano 3 simulation tool. Electrical and magnetic properties of materials like doping concentration, local density of states, Fermi levels and transmission coefficient are focused in this simulation tool nextnano3. Combination of different materials and alloys are characterized for virtual geometry within quantum mechanical environment. The program flow in this software can be explains in [18] summarized way; geometry of devices and material properties of nanostructure can define in a text file along with metal contacts and proper biasing. Proper boundary conditions and structural consideration are also mentioned in that file. Additionally, primarily heterostructure with material constituent are evaluated at given temperature and perform global flow for carrier transport and calculate heavy hole band edges, electrostatic charges, Eigen states of wurtzite and zinc blende structures. Subsequently, current calculation, Schrodinger equation for multiband and Poisson equation are explained for electron transport with self-consistent flow using Contact block reduction technique. Finally, electrical and structural properties can be computed. Similarly, combination of III-V materials and IV group materials with good crystal lattice are utilized from the database of this tool nextnano3 [19-21].

3. Mathematical and Operational Details

The Approach, which was introduced by Landauer in 1988 [22-23] has been used in this paper. Buttiker generalize this approach for multiterminal devices to carrier transport at mesoscopic level [24-25]. Hence, both scientist combine the approach and make them Landauer-Buttiker (LB) formalization for heterostructure and nanodevices. This approach for elastic scattering within ballistic limits is equivalent to Green's function for nonequilibrium level.

3.1. Proposed approach

The proposed technique is Contact block reduction (CBR) which was initially suggested by the scientist Mamaluy [26], is very analogous and resourceful formalization of Green's function for carrier transportation. Open quantum system and its structural and electrical properties has been analyzed with this process i.e. transmission function, space charge density and carrier concentration of carriers within semi-metals and alloys used in these mesoscopic device structure for random number of interactions inside ballistic boundaries.

Firstly, we create a device and meshed it with grid points with N_T number in the real space environment. Now, we create the Hamiltonian Matrix H_o within the size N_T. Finally, this close system is applicable for analysis without contacts. Eigen function of the carriers (Wave function of H_o) and resonant energies with sharp edges (Eigen values of H_o) is carried out by this mesoscopic system. Lastly, Cathode and anode are added to the device and create the discretization with N_c number of grid points with interior point of grid be N_D. So, a sum of grid points in the device would be-

$$N_T = N_C + N_D \quad (1)$$

The grind points in boundary are equal to contact grid points (N_c) of the device which comes under test after connecting the leads of the device. Then these contact leads have connected to get resonant energies broader; then these density of states which are continuous have to alter into separate form of DOS. Above mentioned broadening matrix Γ(E) has depended on Hamiltonian matrix $H_o$of predefined size and required energies. The Self-Energy matrix ∑ (E)will help in calculating the matrix within the Neumann boundaries associated with this device [18].

3.2. DBRTD structure for CBR method

Double barrier heterostructure has been modeled with this CBR method, here geometry of the device is supposed to be regularly varying according to the requirement in (x, y) plane of axis. And transportation of the carrier's will be anticipated in the direction of z-axis. Here, anode and cathode are two leads (i.e. N_a=2) of this defined device for biasing. Device is surrounded with the boundary conditions that are considerably accountable and grids be exactly one (N_a=1). Hence, a sum of grids within the device structure of 41nm be given by-

$$N_C = \sum_{a=1}^{L} N_a = 2 \quad (2)$$

This average calculation of all the factors associated with the device like Density of states, transmission function, Fermi level, charge density, etc. Here, the grid points are taken be two (N_c = 2).

3.3. Device Hamiltonian Energy levels and Wavefunction

Primarily, we calculate for a closed system then analyze the energy bands and wave function of matrix Hamiltonian H^o. Now, Envelop function approximation with dispersion in parabolic form has been taken in account for the calculation of parameters with Schrodinger equation in the device.

The Schrodinger equation can be solved for the hetero-structure which is horizontally challenged in x and y directions and developed along z-direction be-

$$H^o_{k_p}\psi(z,K_p) = E_n(k_p)\psi(z,k_p) \quad (3)$$

Here, wave function is $\psi(z,k_p)$ and it is sub-divided into solution $\psi(z,k_p)$ along the direction of z-axisand plane wave $\exp^{ik_p.r}$ in horizontal (x, y) plane.

$$\psi(z,K_p) = \psi(z,k_p)\exp^{ik_p.r} \quad (4)$$

In above mentioned equations, we flout the requirement of parallel momentum k_p on $\psi(z,k_p)$ of the device. Also, the solution in one dimension of the Schrodinger equation be-

$$H^o\psi_n(z) = E_n\psi_n(z) \quad (5)$$

$$[-\frac{\hbar^2}{2}\frac{\partial}{\partial z}[\frac{1}{m^*(z)}\frac{\partial}{\partial z}]+V(z)]\psi_n(z) = E_n\psi_n(z) \quad (6)$$

Now, $m^*(z)$ be effective mass tangent component along the direction of z-axis, $\hbar$ is Planck's constant with division by 2π, $V(z) = E_c(z) = E_{c,0}(z) - \exp\phi(z)$ is the potential energy spatially. After solving the Poisson's equation, $\phi(z)$ is the electrostatic potential. $E_{c,0}(z)$ is profile of conduction band edge with particular interest counting offsets of material interference.

3.4. Device boundary conditions

The planned nanostructure is discretizing with the help of finite difference technique, which is mentioned in the above equations. At the ends of the device, through the constant grid, device is bounded with Neumann's boundaries. For close system, both the leads are connected and take the results.

Dirichlet's conditions are also applied, but not properly useful over the Neumann boundaries. Wave function within the device has cleared this fact. Dirichlet's conditions don't support the transportation of carrier over the two grid points. But, the property of mimicking in Neumann system is far better for real system in resonant open system wave function.Amplitude of wave functions with constant gridding is fully described with these conditions for fixed numbers of end points.

3.5. Transmission coefficient calculation

This section gives the calculation of transmission coefficient [T_{ab} (E_i)] from one end to other within the device. Broadening matrix ΓC and retarded Green's function G_C^R [18] are the deciding factor for calculation and it is given by this equation.

$$T_{ab}(E_i) = T_r\left[\Gamma_C^a G_C^R \Gamma_C^b G_C^{R^*}\right] \quad (7)$$

Here, leads of the device are named as a & b, and * shows the transpose in conjugate form.

3.6. Computation of Current

Computation of current in this heterostructure with CBR technique with corresponding boundary conditions has been done with the help of these functions like transmission coefficients and Hamiltonian of this bounded system. Scattering with no phase breaking involves the propagation Transmission function within the device as electron transport in it. But, elastic scattering has been interpreted in Hamiltonian (H_o) at truncated temperature and tremendously trivial device identical to RTD.

Electron transport in the DBRTD is coherent and acceptable generally for all nanostructures, with inclusion of relaxed energy of electron and its momentum. Predominantly, a blend of Landauer-Buttiker (LB) validation is proficient and comparable to Green's function validation. With the help of LB formula, the abridged inverted current has been communicated as follows-

$$I_{ab} = \frac{-g_s q}{h}\int T_{ab}(E)[f(E,\mu_a) - f(E,\mu_b)]dE \quad (8)$$

Now, current flowing through the anode and cathode is I_{ab}. T_{ab}(E) is transmission coefficient which is dependent on

the both the contacts. Chemical potential of the device be called as μ_a and μ_b. Energy is gives as E and Planck's constant is referred as h, charge is represented by q and electron spin degeneracy is g.. And Fermi-Dirac function at equilibrium condition within the device is given by-

$$f(E,\mu_a)=\frac{1}{1+\exp[E-\mu_a]/(k_BT)} \quad (9)$$

Here, k_B represents Boltzmann's constant and temperature is termed as T.

3.7. Details of Bands(Conduction & Valance) for material in DBRTD

The two materials,mainly use by this device are GaAs and AlGaAs. The band energies of these materials are explained in table-1 & table-2.These properties are very important for calculation of parameters used in solving equation used in current calculations.

Table-1: Material details of GaAs with band energies

Type of Binary	GaAs-zb-default		
Conduction-bands	3		
Conduction-band-masses	0.670D-01	0.6700D-01	0.67D-01 Γ
	0.190D+01	0.7540D-01	0.754D-01 L
	0.130D+01	0.2300D+00	0.23D+00 X
Degeneracies - conduction-band	2	8	6(including spin degeneracy)
Energies-conduction-band	0.00D+00	0.2960D+00	0.462D+00 [eV]
Valence-bands	3		
Valence-band-masses	0.50D+00	0.500D+00	0.50D+00Γ
	0.680D-01	0.680D-01	0..68D-01L
	0.172D+00	0.172D+00	0.172D+00 X
Degeneracies-valence-band	2	2	2(including spin degeneracy)
Energies-valence-band	-0.1633D+01	[eV]	

4. Proposed Device Model

Double barrier structure of RTD, which is presented above in figure-1, has been proposed in this article. This structure contains 41 nm of quantum well which is developed with altered layer arrangements. Quantum well is squash in the middle of two barriers with inclusion of retardation spacer layer. This two dimensional structure of GaAs/$Al_{0.3}Ga_{0.7}As$with the dimensions at nano-scale, the configuration of the layers is revealed in table-3. Another model has also been introduced with silicon delta doping shown in figure-2 and its layer structure is specified in table-4. To achieve this type of geometry at nanoscale geometries was difficult to fabricate until the crystal-growth at thin-film semiconductor techniques like growth of wafers with molecular beam epitaxy [27-28].

Table-2: Material details of$Al_{0.3}Ga_{0.7}As$ with band energies

Type of Binary	$Al_{0.3}Ga_{0.7}As$		
Conduction-bands	3		
Conduction-band-masses	0.670D-01	0.670D-01	0.67D-01 Γ
	0.190D+01	0.754D-01	0.754D-01 L
	0.130D+01	0.230D+00	0.23D+00 X
Degeneracies-conduction-band	2	8	6(including spin degeneracy)
Energies-conduction-band	0.300D+00	0.3365D+00	0.37515D+0 [eV]
Valence-bands	3		
Valence-band-masses	0.500D+00	0.500D+00	0.500D+00Γ
	0.1256D+00	0.1256D+00	0.1256D+0 L
	0.2044D+00	0.204400D+00	0.2044D+00 X
Degeneracies-valence-band	2	2	2(including spin degeneracy)
Energies-valence-band	-0.17797D+1	[eV]	

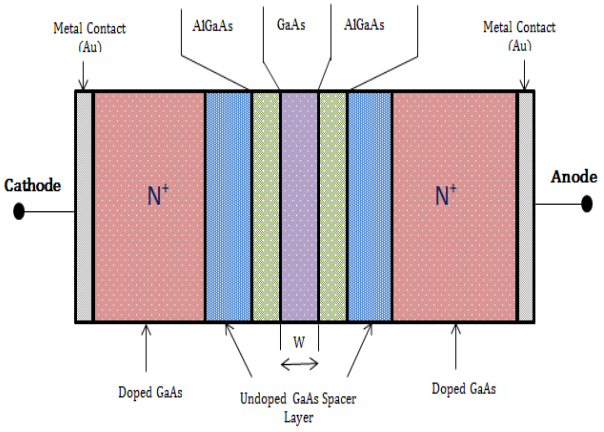

Figure 1: 2D structure of moderately doped Double Barrier RTD

This device has two barrier layers, a quantum well with spacer layers and contacts of the device, shown in the Table-1. The thicknesses of these layers have also given and the 2D structure of mentioned device revealed in fig-1. Fig-2 shows the basic model of delta doped DBRTD. The two dimensional structure of this device is of 10nm width and 41 nm height (10.0 nm x 41.0 nm). The configuration

of layers mentioned above has been simulated and evaluated with the ballistic limits of the device. And Fig.1, which gives the impression that how the device appears after fabrication. To make this DBRTD more compatible with other devices and circuits, we keep into the mind for moderate doping concentration. Table-1 shows the material layers of structure without δ doping and Table-2 shows with δ doping (at center of the well) structure layers detail

Table-3: Layers details of GaAs/ $Al_{0.3}Ga_{0.7}As$ DBRTD at 300°K

S.No.	Material Layers	Size of layers (nm) GaAs/$Al_{0.3}Ga_{0.7}As$
1.	Top contact(Au), metal	Gold (Au) = 0.5 nm
2.	Doping ($1.2*10^{18}/cm^3$)	Doped GaAs = 12nm
3.	Spacer layer	Undoped GaAs = 3nm
4.	Undoped Barrier	$Al_xGa_{1-x}As$ (x=0.3) = 3nm
5.	Undoped Well	GaAs = 4nm
6.	Undoped Barrier	$Al_xGa_{1-x}As$ (x=0.3) = 3nm
7.	Spacer layer	Undoped GaAs = 3nm
8.	Doping ($1.2*10^{18}/cm^3$)	Doped GaAs = 12nm
9.	Bottom contact(Au), metal	Gold (Au) = 0.5 nm

Table-4: Layers details of Si-delta doped GaAs/ $Al_{0.3}Ga_{0.7}As$ DBRTD at 300°K

S.No.	Material Layers	Size of layers (nm) δ-doped GaAs/$Al_{0.3}Ga_{0.7}As$
1.	Top contact(Au), metal	Gold (Au) = 0.5 nm
2.	Doping ($1.2*10^{18}/cm^3$)	Doped GaAs = 12nm
3.	Spacer layer	Undoped GaAs = 3nm
4.	Undoped Barrier	$Al_xGa_{1-x}As$ (x=0.3) = 3nm
5.	Undoped Well	GaAs = 4nm (δ-doping =1 nm)
6.	Undoped Barrier	$Al_xGa_{1-x}As$ (x=0.3) = 3nm
7.	Spacer layer	Undoped GaAs = 3nm
8.	Doping ($1.2*10^{18}/cm^3$)	Doped GaAs = 12nm
9.	Bottom contact(Au), metal	Gold (Au) = 0.5 nm

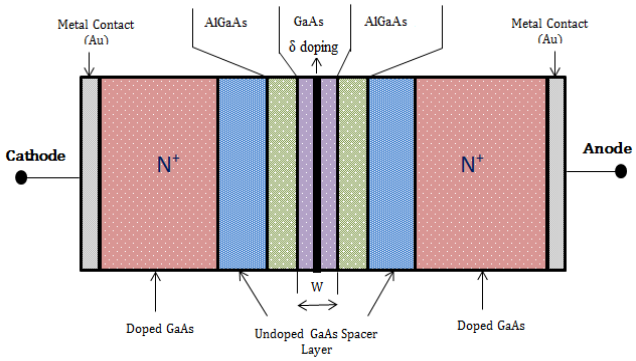

Figure 2: 2D structure of siliconδ-doped GaAs/ $Al_{0.3}Ga_{0.7}As$ Double Barrier RTD

5. Simulation and Electrical Activity

In this section, we simulate the device as defined above in Table-1 and table-2,and then characterize its electrical properties. Firstly, simulation of the device structure then characteristics to plot the chart such as electrostatic potential, energy band gap, Fermi level diagrams, electron density and charge density patterns. Secondly, simulate the Si delta doped DBRTD and characterize the device in terms of current-voltage plots, PVCR ratio and NDR curves. Finally, the variation of device parameters and their effects on these properties has been discussed for both the structures.

5.1. Structural Properties

The structure of the device, as given above, has been simulated to get the plots of physical geometry. Firstly, we have taken the doping concentration of $1.2\times10^{18}/cm^3$with 3nm barrier lengths and 4nm quantum well. Figure-3(a) gives the electrostatic potential generated in GaAs/$Al_{0.3}Ga_{0.7}As$ RTD. According to Poisson's equation, p-type doping sinks the electrons and n-type doping increases the electrostatic potential, thus satisfy the graph plotted.

Here, Electrostatic potential has been calculated 0.05V which satisfy the calculated value. We are comparing these dimensions [24] and reduce the dimensions with getting the better result. Lastly, we simulate same properties of δ doped structure and studied their properties.

Electron density during device has been shown in Figure-3(b) and pattern shows how the electron concentration varied throughout the device at moderate doping concentration and below this concentration device has not been performing the actual phenomenon.

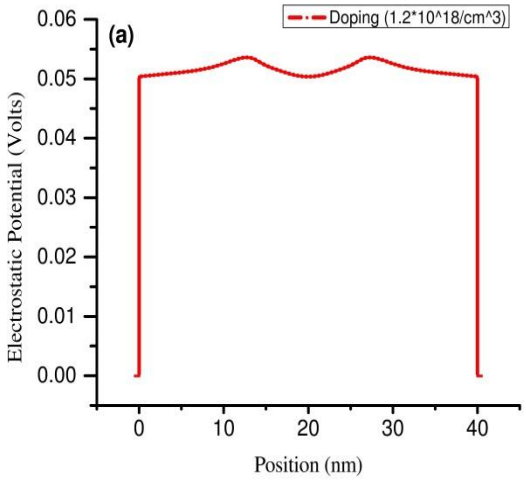

Figure3(a):Simulated plot of Electrostatic Potential throughout the device

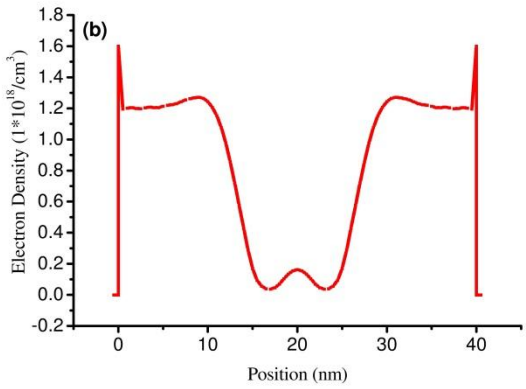

Figure 3(b): Simulated plot of Electron density throughout the device

Figure-4 provides the energies of band gap with the appropriate energies within valance band and conduction band, which calculate the energy of a carrier to transfer from emitter end to collector. Vigard's Law explains the energy of band gap present in materials made with different composition (x) and it is calculated as-

$$E_{g,AlGaAs} = xE_{g,AlAs} + (1-x)E_{g,GaAs} \quad (10)$$

Calculation of band gap energies for this alloy can be done with AlAs and GaAs. Validation of this band gap has been strictly done with comparing the simulation value of RTD (E_g=1.83 eV) and calculated value with this Vigard's law. After validation we can precede this device for additional simulation.

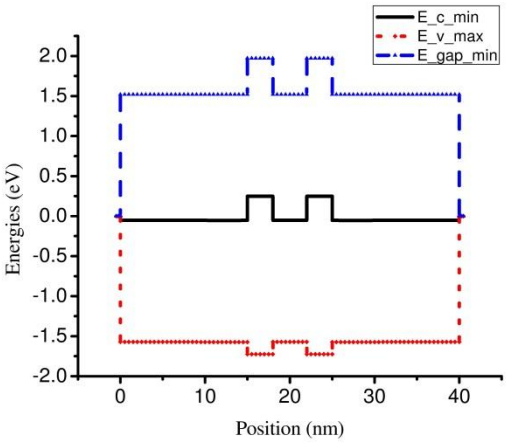

Figure 4: Simulated Energy band gap, conduction and valance band without bias Voltage

The charge densities throughout the device have been simulated in a figure-5. When electron are free to move in spatial direction and energy is quantized in direction perpendicular to spatial direction, referred as Two-dimensional electron gas (2DEG) which is shown in Figure. It also verifies that the concentration profile and charge density is valid for further simulation.

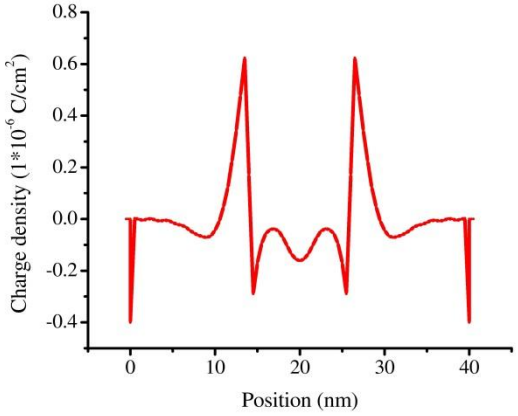

Figure 5.Simulated Space Charge density throughout the device

5.2. Current-Voltage Characteristics

Current-Voltage characteristic of this nanostructure gives the performance execution. Current densities of the device at different device parameters are explained and calculated its extremes' limits. Here,electron transport within the device has been compared to wringer electron transport [29], and achieve the high value of current density between the biasing voltage of 0.3 and 0.5 volts as shown in figure-6.

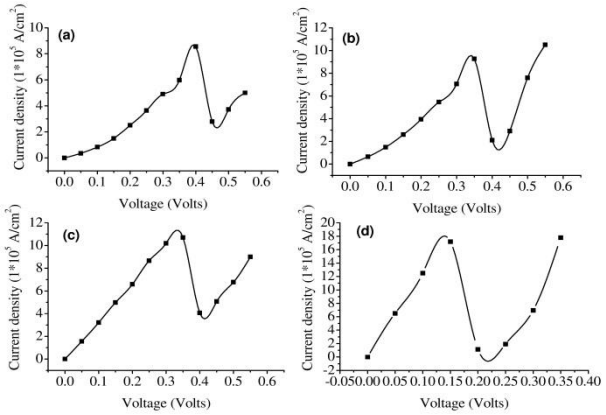

Figure 6:I-V characteristics of Double Barrier RTD at different concentrations of doping (N_D): (a) N_D = 1.2×10^{18}/cm^3, (b) N_D= 2.0×10^{18}/cm^3, (c) N_D = 4.0×10^{18}/cm^3, (d) N_D= 40×10^{18}/cm^3.

5.2.1 Doping Concentration Variation

Figure-6 shows the graph of current density versus operating voltages at various doping concentrations. This variation reaches to its peak limits as shown in graph whether it is maxima or minima. Here, concentration of 1.2×10^{18}/cm^{3}contribute the lowest limit, Double Barrier RTD can't operate below this limit.Subsequently, concentration of doping lies between 2.0×10^{18}/cm^3 to 4.0×10^{18}/cm^{3}gives moderate values which leads to best

for40×10^{18}/cm^{3}and beyond these limits this device doesn't perform the right process.

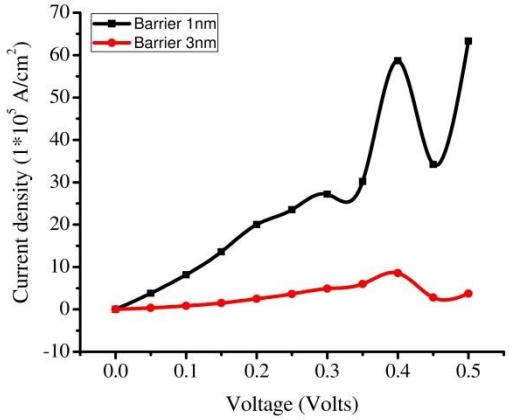

Figure 7:I-V characteristics of GaAs/AlGaAs Double Barrier RTD at different Barrier length

5.2.2 Barrier lengths Variations

For exact carrier transport phenomenon, barrier length is a key factor that play significant role to perform the RTD device properly. Current densities versus voltage graph with varying lengths of barriers are shown in figure-7. On varying collection of barrier length and perform comparison with experimental work [29] to validate the results. Hence, we achieve sharp peaks at 1nm and analyses that on increasing these barriers upto 3nm, current density degrades and very small peaks are achieved.

Here we achieve good PVCR with 1 nm barrier along with very high peak current at moderate concentration of doping. As width of barrier increases to 5nm, the value of current density reaches zero, which means transportation of carrier stop.Hence, maximum limit of barrier length is 3nm for which current flow throughout the device.

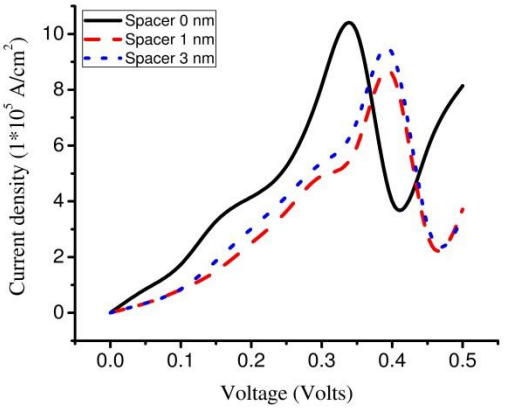

Figure 8:I-V characteristics of GaAs/AlGaAs Double Barrier RTD at varying spacer layer

5.2.3 On varying Spacer layer thickness

A spacer layer in any device relaxes the velocity of an electron and electron reached collector with permissible velocity. If it doesn't happen, the velocity of electron harms the device. J-V characteristics of DBRTD with varying spacer layer are shown in figure-8. As we go beyond 3nm spacer, the current values go down and we cannot measure its actual characteristics. We also compare these variations with 5nm barriers in the given simulated results [30] and get the better peak to valley ratios at different spacer layers.

5.3. Transmission Function at different operating temperatures

The calculation of transmission coefficient T(E) for different operating temperature range of 100K to 400K provide the probability of electron tunnel through the device as shown in figure-9. Transmission coefficient approaches to one at 100K and 400K operating temperature. At room temperature, T(E) degrades its value as compare with other. There is a trade-off between doping and transmission coefficient. So, it is shown on comparing the figure-9 with the figure-10.

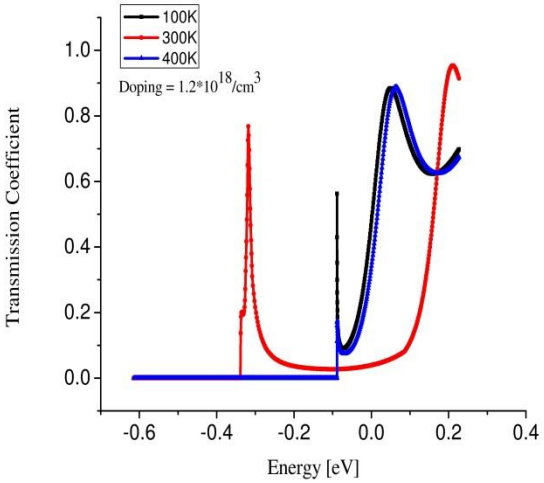

Figure 9: Transmission Coefficient of the device at different operating temperature.

5.4. *Effect of δ-doping* with varying *operating temperatures*

The inclusion of δ doping increase the mobility of the carriers throughout the device. The delta doping is inserted at the center of the well which split the device into two equal proportions and made it symmetric. The current-voltage characteristics are abruptly changes due to this δ doping (2.0×10^{18}/cm^3) which is shown in figure-10 at varying operating temperature. We found that the device is very good at room temperature in comparison to other temperature results. A very good PVCR ratio and multiple peaks are obtained with the help of Si-delta doping at room temperature.

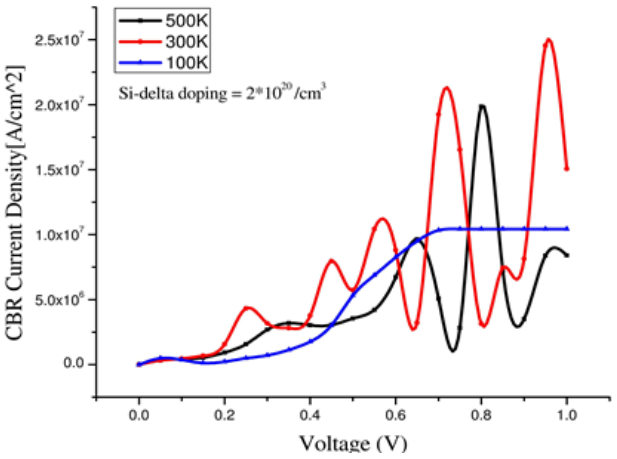

Figure 10: J-V characteristics with Si-δ doping at different temperatures

5.5. Variation of barrier lengths on PVCR

PVCR is an essential parameter of measuring the device performance in any quantum device. Figure-11 shows the barrier length versus PVCR at different doping concentration. Opting of operating points of any device and to minimize the noise margin, a large range of PVCR is required. In addition, large PVCR is also good for application having fast switching, in order to reduce the off-state power dissipation we need low value of valley current. Moreover,as doping increases, PVCR also increases with barrier length. Peak to Valley Current Ratio of the this device can be calculated as-

$$PVCR = \frac{I_P}{I_C} \quad (11)$$

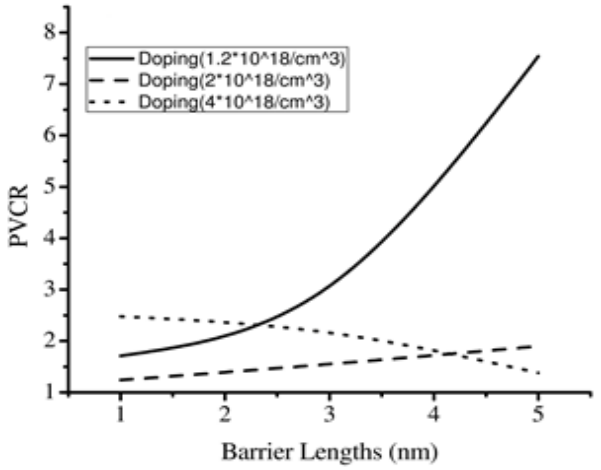

Figure 11: Calculated graph of Barrier length V/sPVCR with varying doping conc. (N_D).

6. Conclusion

Characteristics of GaAs/$Al_{0.3}Ga_{0.7}As$ DBRTD have been analyzed by varying the device parameters. The full device with double barrier has been simulated and validate with the calculated results and almost allconstraints such as electrostatic potential and charge density has been simulated under no bias as well as with varying voltages. Optimization of the device has also been done with calculation of minimum and maximum values for different doping concentration are also being done.

The current density of the device has been affected by current density of sharp peaks, either at maximum and minimum point in support with concentration of doping level. Also, with very high value of doping concentration as shown through simulation, peak current density degrades and get saturate at a doping concentration of $40\times10^{18}/cm^3$ and DBRTDs perform as ordinary tunnel diode. Hence, as we raise the value of doping concentration, peak current increases, simultaneously PVCR of the device increases.

Si-δ doping increases the mobility at various temperatures which is clearly shown in the figures and this doping is $1.2\times10^{18}/cm^3$ and it give high multiple peaks of current densities at various temperatures. Negative Differential Resistance region and PVCR of the device has also been calculated for varying barrier lengths at different doping concentration. Limits for this DBRTD to achieve proper functioning of the device are 5 nm barrier lengths. Some tradeoffs have also been seen, as we increase the doping concentration current will increase, but the device cannot work properly as bias voltage decreased to 0.5 or below.

Acknowledgements

Authors are gratifying to "Council of Scientific and Industrial Research (CSIR)" under Junior Research Fellowship (JRF) scheme (Ref. No. 09/112(0529)/2016-EMR-I) supported by the MHRD, Government of India, New-Delhi. The authors are also grateful to S. Birner, Physics Department, Walter Schottky Institute, Technical University of Munich, Germany for providing us the Nextnano3 simulation package.

References

[1] M. Nagase and T. Tokizaki, IEEE Trans. Electron Devices, Vol. 16, no. 5 (2014), 1321-1326.
[2] Elisa Arduca, Michele Perego, Materials Science in Semiconductor Processing, 64(2017), 156-170.
[3] L. L. Chang, L. Esaki, and R. Tsu, Appl. Physics Letter, Vol. 24 (1974), 593-595.
[4] F. J. Teran et al., EPL-The frontier of Physics, Vol. 85, no. 6 (2009), 67010-67015.
[5] Man Mohan Singh, M. J. Siddiqui, Materials Science in Semiconductor Processing, 58(2017), 89-95.

[6] S. Takagi, A. Toriumi, IEEE Trans. on Electron Devices, Vol. 42, no. 12 (1995), 2125-2130.
[7] Y.C. Yeo, T.J. King, C. Hu, IEEE Transactions on Electron Devices, Vol. 50, no. 4 (2003), 1027-1035.
[8] J. Wang, M. Lundstrom, International Electron Devices Meeting, (2002), 707-710.
[9] H. Kim, S. Yeon, S. Song, S. Park and K. Seo, Japanese J. Appl. Phys., Vol. 45, no. 4B (2006), 3384-3386.
[10] H. Pettenghi, M.J. Avedillo and J. M. Quintana, IEEE Trans. Nanotech., Vol. 10, no. 1 (2011), 155-162.
[11] Man Mohan Singh, M. J. Siddiqui, Inter. IEEE Conf. EDSSC, Vol. 12 (2016), 30-34.
[12] A. Pfenning, F. Hartmann, M. Rebello Sousa Dias, L.K. Castelano,C. Submeier, F. Langer, S. Hofling, M. Kamp, G.E. Marques, L. Worschech, et al., ACS nano, Vol. 9, no. 6 (2015), 6271-6277.
[13] Man Mohan Singh, M. J. Siddiqui, Int. J. Emerging Advan. Electro. Elect. Engg., Vol. 01, (2016), 07-13.
[14] W. Lu, C.M. Lieber, Nature materials, Vol. 6, no. 11 (2007), 841-850.
[15] Man Mohan Singh, M J Siddiqui and A. Saxena, Procedia computer science, Elsevier, Vol. 85 (2016), 581-587.
[16] A. Taube, J. Kaczmarski, R. Kruszka, J. Grochowski, K. Kosiel, K. Golaszewska-Malec, M. Sochacki, W. Jung, E. Kaminska, and A. Piotrowska, Solid-State Electronics, Vol. 111(2015), 12-17.
[17] M. Bhattacharya, J. Jogi, R. Gupta, and M. Gupta, IEEE Tran. Nanotechnology, Vol. 12, no. 6 (2013), 965-970.
[18] S. Birner, C. Schindler, P. Greck, M. Sabathil and P. Vogl, Vol. 8, no. 3 (2009), 267-286.
[19] http://www.wsi.tum.de/nextnano3.
[20] http://www.nextnano.de.
[21] M. M. Singh, M. J. Siddiqui, A. B. Khan, S.G. Anjum, IEEE Spon. Int. Conf. INDICON, Vol. 12 (2015), 1-5.
[22] R. Landauer, IBM J. Res. Develop., Vol. 32, no. 3 (1988), 306-316.
[23] R. Landauer, "Conductance from transmission: common sense points", Phys. Scr., Vol. T42 (1992), 110.
[24] M. Büttiker, "Four-terminal phase-coherent conductance", Phys. Rev. Lett., Vol. 57, no. 14 (1986), 1761-1764.
[25] M. Büttiker, "Symmetry of electrical conduction", IBM J. Res. Develop., Vol. 32, no. 3 (1988), 317-334.
[26] D. Mamaluy, M. Sabathil and P. Vogl, J. Appl. Phys., Vol. 93, no. 8 (2003), 4628-4633.
[27] M. M. Singh, M.J. Siddiqui, A.B. Khan and C.K. Thaseena, IEEE Inter. Conf. IMPACT, Vol. 3 (2013), 264-267.
[28] A.Y. Cho, Thin Solid Films, Vol. 100, no. 4 (1983) pp. 291_317, Feb. 1983.
[29] V. Sharma, R. P. Sharma, Inter. J. Engineering and Comp. Sci., Vol.2, no. 12 (2013), 3580-3583.
[30] P. D. Yoder, M. Grupen, R. K. Smith, IEEE Trans. Electron Device, Vol. 57, no. 12 (2010), 3265-3274.